Measurements of forces acting on suspended microparticles in the void region of a complex plasma

E. Thomas, Jr.*
Department of Physics, Auburn University, Auburn, Alabama 36849

B. M. Annaratone, G. E. Morfill, and H. Rothermel
Max Planck Institut für extraterrestrische Physik, Garching, Germany
(Received 18 February 2002; published 25 July 2002)

A laboratory experiment has been performed in which a temperature gradient is used to generate a large central void in a rf-generated complex plasma. Through the use of laser flashing techniques, two-dimensional velocity vectors have been obtained from particles falling from the top to the bottom of the void. These particles are used to generate a two-dimensional map of the acceleration, and consequently the net forces, that act upon particles in the void.

DOI: 10.1103/PhysRevE.66.016405 PACS number(s): 52.27.Lw, 52.80.Hc, 52.25.Fi

I. INTRODUCTION

In the past decade, complex plasmas—a plasma environment consisting of ions, electrons, neutrals, and charged microparticles—have been become a topic of great interest to the plasma physics community [1–6]. Of particular recent interest is the presence of void regions in complex plasmas [7–10]. These are regions in which there is an absence or significant reduction in the number of suspended microparticles. One major factor driving this interest is the appearance of voids under microgravity conditions [11]. Recent ground-based experiments in which a temperature gradient is applied to a complex plasma have been able to qualitatively reproduce similar void structures [12]. However, due to the lack of readily available diagnostics—especially for the microgravity experiments—there are few direct measurements of the properties of these voids.

An experiment is performed to attempt to reconstruct the acceleration and net force acting upon individual microparticles in the void region of a complex plasma. In the experiment, the observed trajectories of single microparticles that fall through the void are used to create a two-dimensional velocity map. From this spatial velocity map and the known properties of the microparticles, a two-dimensional model of the forces acting on particles within the void is constructed.

II. EXPERIMENTAL SETUP

The experiment is performed using the plasma crystal experiment (PKE) chamber [13]. The PKE chamber uses a 13.56-MHz radio-frequency (rf) source to generate argon plasmas between a powered lower electrode and a grounded upper electrode. The neutral pressure in the chamber is maintained at $p = 61$ Pa. The complex plasma consists of suspended 3.4-μm-diameter melanine-formaldehyde spherical microparticles.

For these experiments, a temperature difference is maintained between the upper electrode ($T_1 = 21.9\,^{\circ}\mathrm{C}$) and the lower electrode ($T_2 = 60.8\,^{\circ}\mathrm{C}$) through the use of Peltier elements which maintained a constant temperature on each electrode. The two electrodes are separated by a distance of 30 mm. The application of this temperature gradient across the experimental region has the effect of generating a large, central void region. Figure 1 shows the formation of a void region at the center of the complex plasma. The void is an elliptical region (in two dimensions) with a horizontal major radius $a = 6.75$ mm and a vertical minor radius $b = 3.5$ mm.

The particles are illuminated using a continuous wave diode laser that is expanded into a vertically oriented light sheet using a cylindrical lens. A charge coupled device (CCD) camera, oriented perpendicularly to the light sheet, views a 20 mm (1028 pixels horizontal) by 15 mm (772 pixels vertically) region of the complex plasma. The camera captures images with a 15-frame-per-second rate.

Once the complex plasma is formed in the PKE chamber, the rf power is lowered. As the power is lowered, individual microparticles fall from the upper boundary of the void region, through the void, and reenter the complex plasma through the lower boundary of the void. It is noted that this process causes only a few particles to fall through the void at any given time, allowing each particle to be separately identified and tracked as it falls through the void region.

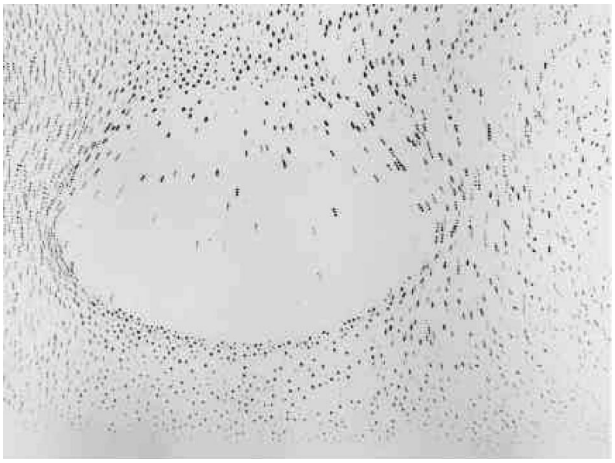

FIG. 1. The formation of the void in the PKE chamber. Particles are shown falling through the void from the upper boundary.

*Email address: etjr@physics.auburn.edu

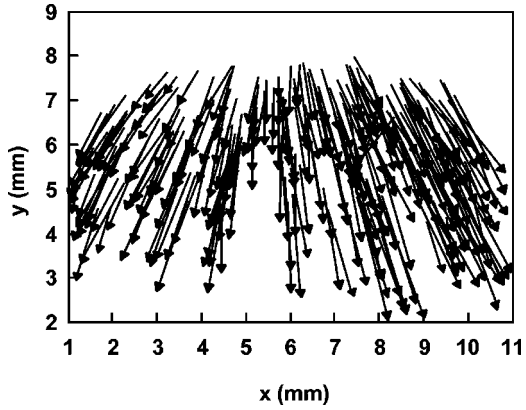

FIG. 2. A mapping of the velocity vectors of particles falling through the void. The velocity vectors are obtained using the laser flashing technique.

In order to measure the velocity vectors of the particles falling through the void, a laser flashing technique was developed. In this technique, the output of the diode laser can be modulated using a pulse sequence. The pulse sequence used allowed the laser output to be modulated to provide 1 msec of illumination with 24 msec interval between each illumination. Because the CCD camera and the laser pulses were not synchronized, each video frame (~67 msec in duration), would capture either two or three of the laser pulses. This laser flashing technique allows individual particles to be identified in each video frame and the spacing between the two or three spots allows a measurement of the particle velocity to be made.

Great care is taken to ensure that the entire void region is mapped. This requires the analysis of many video frames—in this case over one hundred frames. From the measurement of the particle velocities, a two-dimensional model of the horizontal and vertical velocities is generated. The model is then used to generate an estimate of the acceleration (forces) acting on the particles in the void.

III. MEASUREMENT AND ANALYSIS

A mapping of the velocity vectors generated from the laser flashing technique is shown in Fig. 2. This is a reduced set of all of the velocity vectors obtained from the measurement sequence. It is generally observed that the particles all flow downward from the top of the void to the bottom. It is also observed that there is a general spreading of the particles, which indicates the presence of a net outward force acting upon the particles—notably in the horizontal direction. A more detailed analysis, presented below, of the velocity distribution is used to construct a simple two-dimensional model for the particle velocities.

The spatial distributions of the magnitude of the velocity, and the vertical component (v_y), and horizontal component (v_s) of the dust particle velocities are shown in the contour plots in Fig. 3. Both the magnitude of the velocity and the vertical component of the velocity appear to indicate a general and continuous increase in the particle velocity as the particles fall through the void. In the horizontal direction,

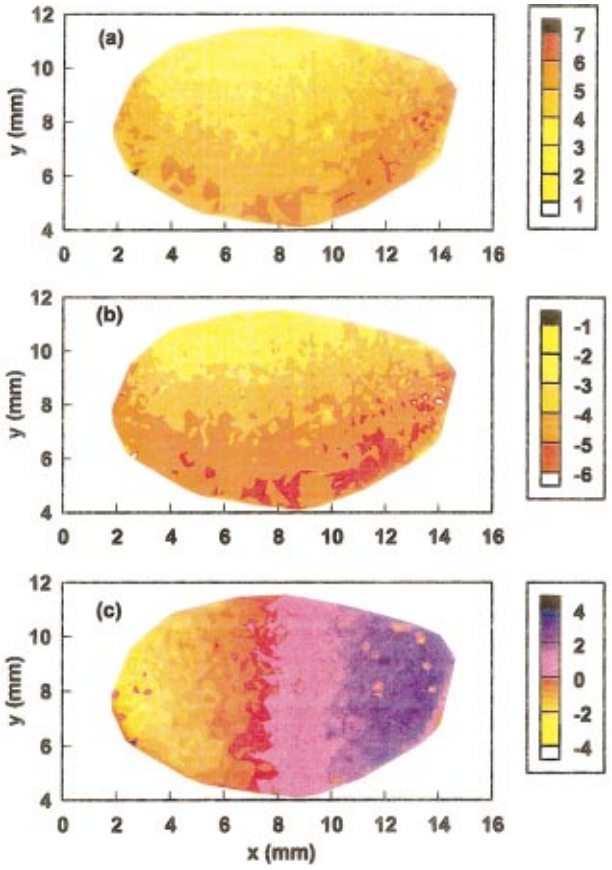

FIG. 3. (Color) Experimental measurements of the spatial distribution of particle velocities measured in the void. (a) Magnitude of the velcity, (b) the vertical component (ν_s) of the velocity. The magnitude of the velocity is given in units of mm/s. The legend to the right of each figure indicates the range of velocities.

there is a strong asymmetry in the measured particle velocities—indicating the presence of an outward pointing force.

In an attempt to understand the forces that led to the observed velocity distributions, a model is generated for the horizontal and vertical velocities. For this model, the region within the last 50–100 μm of the void boundary is not considered since the particle transport in that region is dominated by a rapid deceleration of the particles. This motion will be discussed in a future report.

First, a model for the void region is developed assuming the void is an ellipse. The equation for the structure of the void is then given by

$$\frac{(x-8.0)}{6.75}+\frac{(y-7.7)}{3.5}=1. \tag{1}$$

The point $(x_0,y_0)=(8.0\text{ mm},7.7\text{ mm})$ is the observed center of the void for all of the video images used in this analysis. All subsequent calculations will be restricted to this region.

In the horizontal direction, the horizontal velocity along the line $y=7.7\pm0.2$ mm is considered. This data is shown in Fig. 4(a) where the horizontal axis is the horizontal position in millimeters and the vertical axis is the horizontal velocity

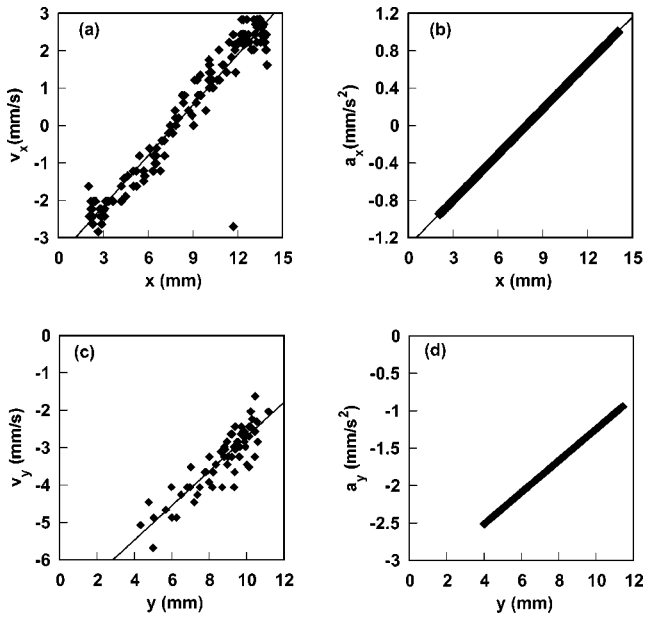

FIG. 4. (a) The horizontal velocity along the line $y=5.5\pm0.1$ mm where the horizontal axis is the horizontal position in millimeters and the vertical axis is the horizontal velocity in mm/s. The solid line is a linear fit to the velocity data as a function of the horizontal position. (b) Shows the model for the horizontal acceleration—a_x in units of mm/s^2—which is computed from the horizontal velocity profile. The horizontal axis is the horizontal position in millimeters and the vertical axis is the horizontal acceleration in mm/s^2. (c) The vertical velocity along the line $x=5.5\pm0.2$ where the horizontal axis is the vertical position in millimeters and the vertical axis is the vertical velocity in mm/s. The solid line represents a second order polynomial fit to the vertical velocity data. (d) Shows the model for the vertical acceleration—a_y in units of mm/s^2—which is computed from the vertical velocity profile. The horizontal axis is the vertical position in millimeters and the vertical axis is the horizontal acceleration in mm/s^2.

in mm/s. The solid line in Fig. 4(a) is a linear fit to the velocity data as a function of the horizontal position. It is assumed that the functional dependence of $v_{x(x)}$ will be maintained throughout the entire void region.

Figure 4(b) shows the model for the horizontal acceleration—a_x in units of mm/s^2—that is computed from the horizontal velocity profile. The horizontal axis is the horizontal position in millimeters and the vertical axis is the horizontal acceleration in mm/s^2. It indicates that the horizontal acceleration is roughly symmetric about the line $y=5.5$ mm—the vertical midplane of the void.

In a similar way, the vertical velocity along the line $x=8.0\pm0.2$ mm is considered and is plotted in Fig. 4(c). Here, the solid line represents a second order polynomial fit to the vertical velocity data. The horizontal axis is the vertical position in millimeters and the vertical axis is the vertical velocity in mm/s. As is done for the horizontal velocity, the functional dependence of $v_y(y)$ is assumed to be valid over the entire void.

The vertical acceleration, a_y, is computed and shown in Fig. 4(d). The horizontal axis is the vertical position in millimeters and the vertical axis is the vertical acceleration in mm/s^2. Here, it is shown that there is a variation in the vertical acceleration as the particles fall through the void. Near the top of the void (at $y=8$ mm), there is an initial vertical acceleration that increases as the particles fall through the void. Like the horizontal acceleration, the vertical acceleration continues to increase uniformly as the particle moves through the void region.

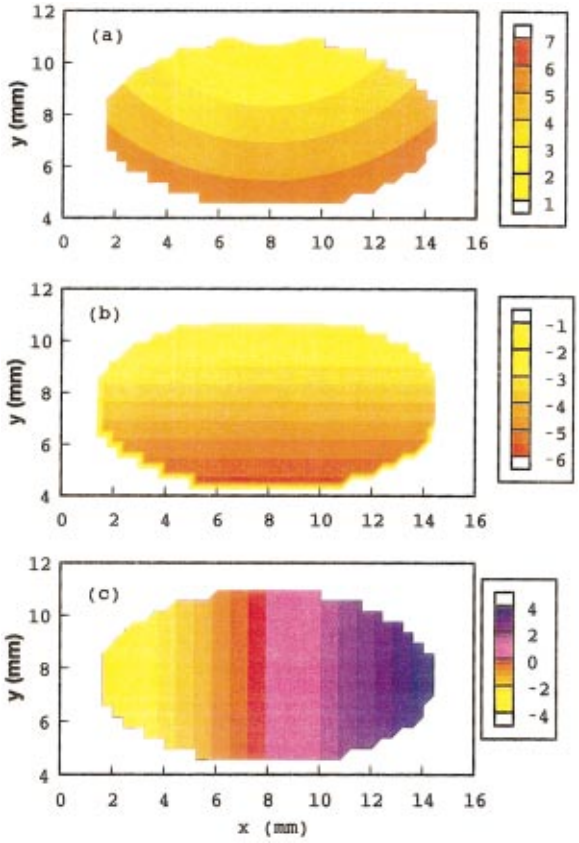

FIG. 5. (Color) Two-dimensional spatial maps of (a) magnitude of the velocity, (b) the vertical component (v_y) of the velocity, (c) and horizontal component (v_x) of the velocity. In each case, the horizontal axis is the horizontal position in millimeters and the vertical axis is the vertical position in millimeters. The model values and spatial structure for the velocity are, in general, good agreement with the experimentally measured quantities.

Using these models for velocity and acceleration, two-dimensional contour plots of the velocity and acceleration over the void region are produced. First, in Fig. 5, are shown two-dimensional spatial maps of (a) the magnitude of the velocity, (b) the vertical component (v_y) of the velocity, (c) and the horizontal component (v_y) of the velocity using the same contour plotting procedures as in Fig. 3. It is observed that the model values and spatial structure for the velocity are in generally good agreement with the experimentally measured quantities.

Based upon this agreement in the two-dimensional velocity profiles, a two-dimensional profile of the acceleration is computed. This is shown in Fig. 6. Figure 6(a) shows a mapping of the acceleration vectors, Fig. 6(b) shows a contour plot of the magnitude of the acceleration, and Fig. 6(c) shows a contour plot of the magnitude of the total force that acts upon the particles.

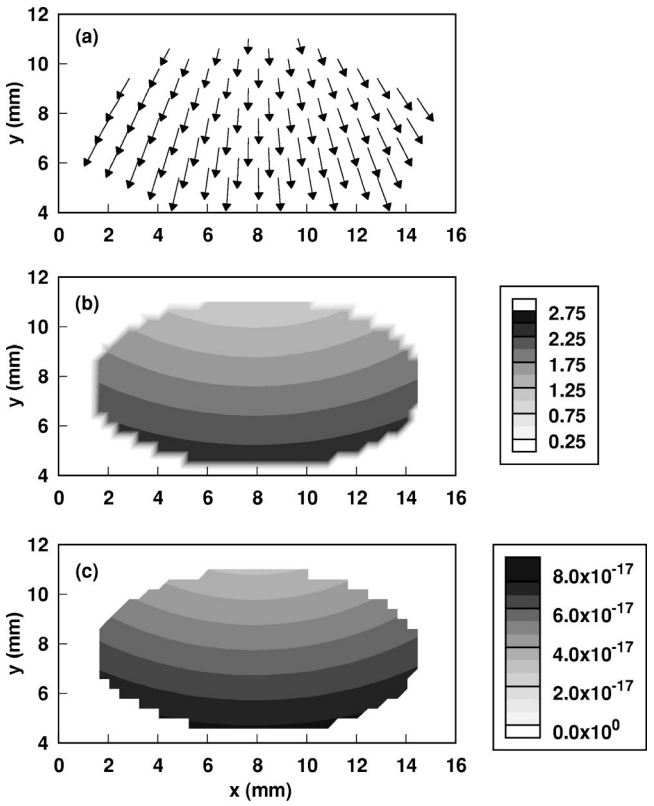

FIG. 6. Two-dimensional spatial maps of (a) the acceleration vectors, (b) a contour plot of the magnitude of the acceleration in units of mm/s^2, and (c) a contour plot of the magnitude of the total force that acts upon the particles. In each case, the horizontal axis is the horizontal position in millimeters and the vertical axis is the vertical position in millimeters. The legend on the contour plots indicates the particle acceleration in mm/s^2 or force in Newtons.

There are several observations that can be extracted from this acceleration profile. First, is the presence of a substantial force in the horizontal direction. This force is responsible for the spreading of the particles as they leave the upper boundary of the void. However, many models of the potential structure between the rf electrodes generally show a uniform electric potential in the regions between the two electrodes [11]. Thus, a major unresolved question is the mechanism that establishes the outward horizontal force.

Another unresolved issue centers on the apparent continuous acceleration experienced by a particle as it transits the void region. This is a somewhat unexpected result because it is unclear what is the physical mechanism that would be responsible for providing the net force on the particle.

IV. DISCUSSION

For the aforementioned experimental conditions ($p=61$ Pa, $\Delta T=38.9\,^{\circ}$C, $\Delta x=30$ mm, $m_p=3.1\times10^{-14}$ kg, $v_p\sim5$ mms, $r_p\sim1.7$ μm, argon gas), several forces contribute to the dynamical equilibrium. Among them we have

$$m\vec{a}=k_E\vec{\nu}+q\vec{E}+\vec{F}_{\text{ion-drag}}+m\vec{g}+\vec{F}_{\text{thermophoresis}}. \qquad (2)$$

Here, qE_{elec} is the electric force, $m\vec{g}$ is the gravitational force, $m\vec{d}$ is the inertia term—which is determined experimentally, $F_{\text{ion-drag}}$ is the ion drag force, $F_{\text{thermophoresis}}$ is the thermophoresis force—the force due to the temperature gradient in the gas, and k_Ev is the neutral drag term where k_E is the reflexive value of the Epstein coefficient, $k_E=5.18\times10^{-12}$. Among the key parameters that are not determined experimentally are the microparticle charge q and the electric field in the plasma.

The first two of these forces are known from the above experiments. They both are linear in the space coordinate and fully symmetric around the center of the void in the horizontal direction. It is noted that the maximum value of the inertia term ($m\vec{a}\sim7.8\times10^{-17}$ N) is much smaller than the neutral drag term, $k_Ev=3.9\times10^{-14}$ N. This suggests that acceleration is being determined by a small imbalance among the other, larger forces. Furthermore, this also suggests that the particle motion is strongly damped within the main particle cloud where there exists an equilibrium among the forces. This explains why all the particles have, within a limited range, the same velocity regardless of their entry point to the void.

A. Horizontal component

Since Eq. (1) is a vector equation, it is necessary to consider each vector direction separately. First, in the horizontal direction, there is neither gravity nor the applied thermophoresis. Therefore, the sum of the two experimentally measured forces—the inertia term ($m\vec{a}$) and neutral drag (k_Ev)—will be equal to the sum of the electrostatic (qE) and ion drag ($F_{\text{ion-drag}}$) terms. It is noted that although the electrical potential structure in the void is mainly unknown, it is reasonable to assume a presheath potential, of the order kT_e/e, as in the usual wall-surrounded plasmas. Assuming that the particle charge remains constant and that the momentum transfer cross section for the ion collision is independent of the energy, the ion drag and electrostatic force terms will both be directly proportional to the electric field.

A plot of experimentally measured term $m\vec{a}_x-k_Ev_x$ and the total electrostatic term ($\xi E_x=qE_x+F_{x\text{-ion-drag}}$) is shown in Fig. 7(a). This plot shows that this term, and consequently the horizontal component of the electric force, is symmetric and linear in the horizontal direction. Thus, the negatively charged microparticles would be pushed inward towards the center of the void and the ion drag force would push the microparticles outward. The observed net outward acceleration in the horizontal direction suggests that the ion drag force is dominant in the horizontal direction.

B. Vertical component

In the vertical direction, interpreting the experimental results is more complex because of the presence of the gravitational and thermophoresis forces. From microgravity experiments, it has been shown that there is both an outward symmetric horizontal and vertical force [14]. The microgravity experiments are performed in the absence of an applied thermophoresis force and, of course, gravity. However, in the

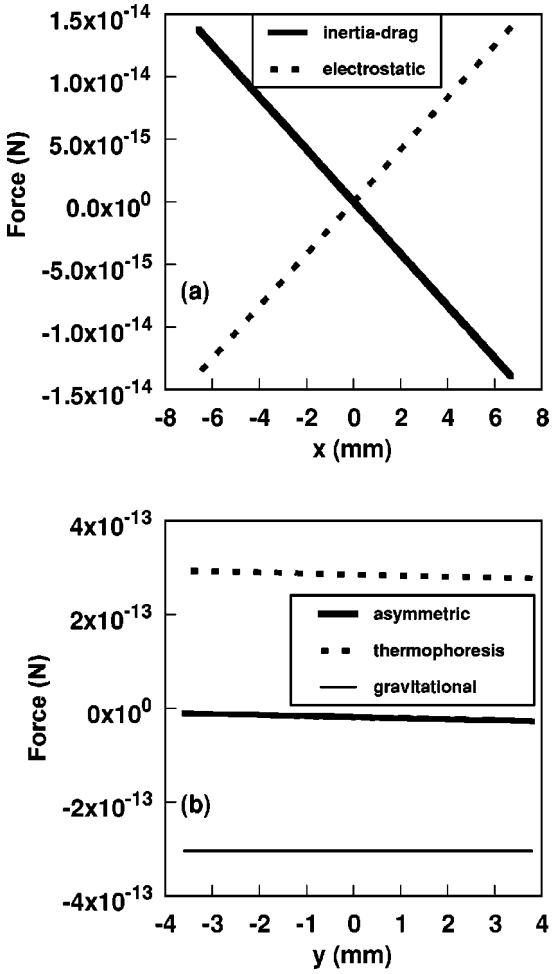

FIG. 7. (a) Comparison of the experimentally measured term $m\vec{a}_x - k_E v_x$ (solid line) and the electrostatic term (dashed line). The plot shows that these terms are symmetric and linear in the horizontal direction. (b) Comparison of the asymmetric (thick solid line), gravitational (thin solid line), and thermophoresis terms (dashed line). The plot shows a slight nonhomogeneity in the value of the thermophoresis force with the force being slightly weaker at the top (positive y values) of the void.

ground-based laboratory studies, the gravitational and thermophoresis forces break this symmetry. Thus, symmetric and nonsymmetric components of the vertical forces are considered.

First, the symmetric components are examined. Following the analysis of the horizontal components, it is expected that the combination of the electrostatic force and ion drag terms will be linear in the electric field. Furthermore, it will be assumed—based upon the results of the microgravity studies—that these forces are symmetric in both the horizontal and vertical directions. These symmetric forces would lead to a vertical velocity profile that, in the absence of the gravitational and thermophoresis forces, would have the same spatial structure as the horizontal component, i.e., scaling with the void dimensions as in Ref. [14]. The model for the symmetric velocity in the vertical direction is then given by Eq. (3). Here β_x and β_y are the slopes of $v_x(x)$ and $v_y(y)$, respectively, and Δx and Δy represent the spatial extent of the void in the horizontal and vertical directions:

$$\nu_x = \beta_x x \quad \nu_y^{\mathrm{sym}} = \beta_y y$$

$$\frac{\beta_y}{\beta_x} \sim \frac{\Delta x}{\Delta y} \sim \frac{6.75}{3.5}. \tag{3}$$

The y-component of Eq. (2) is then reordered to obtain

$$[m\vec{a}_y - k_E \nu_y^{\mathrm{asym}} - (m\vec{g} + F_{\mathrm{thermophoresis}})] - [k_E \nu_y^{\mathrm{sym}} + \xi E_y] = 0, \tag{4}$$

where the term in the first bracket represents the asymmetric components and the term in the second bracket represents the symmetric components. All of the electrostatic effects, both the electrostatic and ion drag forces, are included in the term ξE_y.

Consequently, for the asymmetric components, the term $k_E v_y^{\mathrm{asym}}$ will be computed from the difference $(k_E v_y - k_E v_y^{\mathrm{sym}})$. Therefore, since the gravitational force is known $(m\vec{g} = -3.05 \times 10^{-13}$ N) and the inertia term is measured experimentally, it is now possible to estimate $F_{\mathrm{thermophoresis}}$. The average value of the thermophoresis is 2.85×10^{-13} N. The thermophoresis also shows a $\sim$5.5% nonhomogeneity, with the force being slightly weaker in the upper part of the void. This apparent variation in the thermophoresis may account for the convective flows that are often observed at the edges of the void region; i.e., an upward flow of particles from below the void and a returning downward flow from above the top of the void region. A comparison of the gravitational, thermophoresis, and total asymmetric force is shown in Fig. 7(b).

This value is compared against a calculation of the thermophoresis force using the experimentally determined parameters for the PKE chamber presented by Rothermel, *et al.* [12]. Here, the thermophoresis is computed from $F_{\mathrm{thermophoresis}} = -2.26 r_p^2 (\sqrt{2}\Lambda / 1.2 v_{\mathrm{th}})(dT/dx)$. Here, Λ is the thermal conductivity (1.11×10^{-2} W/mK for argon), r_p is the radius of the microparticle ($r_p = 1.7 \times 10^{-6}$ m), and v_{th} is the thermal velocity of the argon atoms in the gas ($v_{\mathrm{th}} = \sqrt{8 k_B T / \pi m}$; k_B is Boltzmann's constant, T is the temperature of the gas, and m is the atomic mass of the gas). The term (dT/dx) is the temperature gradient which corresponds to 1297 K/m for these experimental conditions. The resulting thermophoresis force is $F_{\mathrm{thermophoresis}} = 2.73 \times 10^{-13}$ N, $\approx$4.3% lower than the average value computed above.

The close agreement between these two methods of computing the thermophoresis force suggests that the method of decomposing the forces into symmetric and asymmetric components is a valid approach for interpreting these experimental measurements. This also suggests that the assumption of a linear temperature gradient in the PKE chamber is valid.

Additionally, this analysis technique of reordering the forces in terms of electrostatic forces, drag forces, etc., offers an alternative method of interpreting the observed particle dynamics in laboratory or microgravity complex plasma experiments in which direct measurements of experimental parameters are difficult.

C. Work done on the microparticles

With estimates of the forces present in the horizontal and vertical directions, the work done on the microparticles in their motion through the void can be computed. Here, the horizontal force and the symmetric component of the vertical force are considered. The work is computed by starting a microparticle at the center of the void region with zero energy and allowing the particle to move in either the horizontal or the vertical direction towards to the void boundary. A plot of the work done on the microparticles is shown in Fig. 8.

In Fig. 8(a), the work is shown for a microparticle that is moved horizontally outward from the center of the void in the positive x direction. In Fig. 8(b), the work is shown for a microparticle that is moved vertically outward from the center of the void in the positive y direction. The solid line in Fig. 8(b) is the work done on the microparticle by the symmetric forces and the dashed line is the total work done. It is noted that for these ground-based experiments, the total work done by the upward moving microparticle is negative as a result of the net downward force. Under microgravity conditions, the work done by symmetric force would be apparent.

It is noted that the forces are not conservative because the work done by the symmetric forces in x and y to reach the boundary are different. The boundary is presumably an equipotential surface. In the x direction, $W_x \sim 0.7$ eV is required to travel 7 mm to the boundary whereas in the y direction, $W_y \sim 1.2$ eV is required. This is not unexpected due to the presence of dissipative forces, such as the neutral drag and ion drag, in the experiment.

While some important information has been extracted from these measurements, it is clear that new, noninvasive diagnostic techniques need to be developed to obtain measurements of various quantities in these experiments. Among them are the microparticle charge—notably, determining what the charge is and if screening of the charge is a factor, to resolve the roles of the ion drag and electrostatic forces, the potential structure at the interior of the void and at the void boundary, and the temperature gradient, in order to better understand the role of convection.

Finally, one of the more intriguing aspects of these measurements is the persistence of the void structure. Irrespective of whether the void has a positive or negative potential structure, it is important to note that the void structure is completely stable. This suggests that a source of particles, e.g., ions and electrons, because of enhanced ionization in the center of the void, or energy needs to be present at the center of the void structure in order to maintain its spatial structure. Experimentally, it is unclear what physical mechanisms lead to the formation and persistence of the void and why the void generally forms at the geometric center of the PKE chamber.

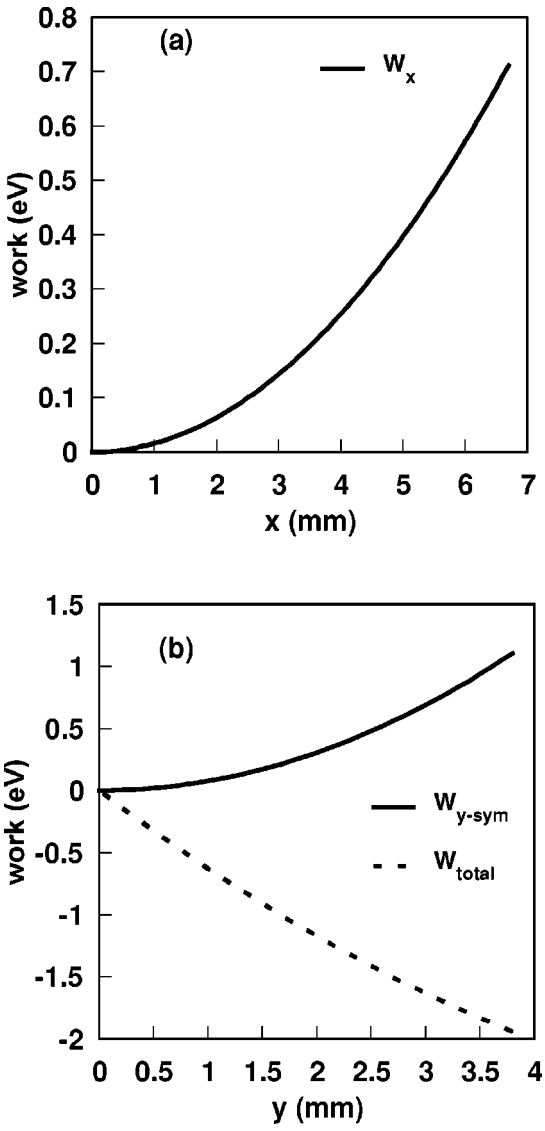

FIG. 8. Calculation of the work done on a microparticle that starts at the center of the void and travels either horizontally or vertically to the boundary. (a) Work is shown for a microparticle that is moved horizontally outward from the center of the void in the positive x direction. (b) Work is shown for a microparticle that is moved vertically outward from the center of the void in the positive y direction. The solid line is the work done on the microparticle by the symmetric forces and the dashed line is the total work done.

V. SUMMARY

In summary, an experiment has been performed to characterize the forces that act upon particles in the void region of a complex plasma. A void in an rf-generated complex plasma is produced in a laboratory experiment with an externally applied temperature gradient. Laser flashing techniques are used to identify the particles and to

obtain two-dimensional maps of the particle velocities. From these measurements, two-dimensional maps of the acceleration and force acting upon particles in the void are computed.

The results indicate that the particles undergo continuous acceleration as they move through the void region. In the horizontal direction, a substantial, spatially symmetric outward force accelerates the particles. In the vertical direction, the presence of gravitational and thermophoresis forces break the symmetry of the experiment. A decomposition of the vertical motion into symmetric and asymmetric components allowed an estimate of the average thermophoresis force to be made. This value compares favorably with an estimate computed from the assumption of a linear temperature gradient across the experimental region. Additional detailed measurements of the temperature gradients and particle charges are needed to fully understand the dynamics within the void.

ACKNOWLEDGMENTS

This work was supported by Grant No. PHY-0096254 from the National Science Foundation. Additional support for this project was provided by the Auburn University Physics Department and College of Science and Mathematics. One of the authors (E.T.), would like to express his gratitude to the members of the Max Planck Institut für extraterrestrische Physik for the use of the PKE chamber and their hospitality during his visit to MPE. The PKE chamber was designed in context with a space research project funded by Das Bundesministerium für Bildung und Forschung durch das Zentrum für Luft- und Raumfarht e.V. (DLR), Förderkennzeichen 50WB9852.

[1] J. H. Chu and Lin I, Phys. Rev. Lett. **72**, 4009 (1994).
[2] H. M. Thomas and G. E. Morfill, Nature (London) **379**, 806 (1994).
[3] H. Thomas, G. E. Morfill, V. Demmel, J. Goree, B. Feuerbacher, and D. Möhlmann, Phys. Rev. Lett. **73**, 652 (1994).
[4] A. Melzer, T. Trottenberg, and A. Piel, Phys. Lett. A **191**, 301 (1994).
[5] Y. Hayashi and K. Tachibana, Jpn. J. Appl. Phys., Part 2 **33**, L804 (1994).
[6] R. A. Quinn, C. Cui, J. Goree, J. B. Pieper, H. Thomas, and G. Morfill, Phys. Rev. E **53**, R2049 (1996).
[7] K. Avinash, Phys. Plasmas **8**, 2601 (2001).
[8] V. N. Tsytovich, S. V. Vladimirov, G. E. Morfill, and J. Goree, Phys. Rev. E **63**, 056609 (2001).
[9] V. N. Tsytovich, Phys. Scr., T **T89**, 89 (2001).
[10] G. Praburam and J. Goree, Phys. Plasmas **3**, 1212 (1996).
[11] G. E. Morfill, *et al.*, Phys. Rev. Lett. **83**, 1598 (1999).
[12] H. Rothermel, T. Hagl, G. Morfill, and H. Thomas (unpublished).
[13] The plasma crystal experiment (PKE) chamber used for this experiment is a duplicate of flight hardware that was used on board the International Space Station from March 1, 2001 through March 21, 2001.
[14] M. Kretschmer and U. Konopka (private communication).